Effect of phase separation on the kinetics of photocurrent relaxation in Sn–Sb–Se glassy films

2009 J. Phys.: Condens. Matter 21 375102

(http://iopscience.iop.org/0953-8984/21/37/375102)

J. Phys.: Condens. Matter **21** (2009) 375102 (6pp) doi:10.1088/0953-8984/21/37/375102

Effect of phase separation on the kinetics of photocurrent relaxation in Sn–Sb–Se glassy films

Praveen Kumar and R Thangaraj

Semiconductors Laboratory, Department of Applied Physics, Guru Nanak Dev University, Amritsar 143005, India

E-mail: rthangaraj@rediffmail.com

Received 9 February 2009, in final form 27 May 2009
Published 11 August 2009
Online at stacks.iop.org/JPhysCM/21/375102

Abstract

The effects of phase separation on the structure and photoconductivity kinetics in $Sn_xSb_{20}Se_{80-x}$ ($x = 10, 11, 12.5$) glassy films have been studied. Crystalline peaks for $SnSe_2$, $Sn_2Sb_4Se_8$ and $Sn_4Sb_4Se_{10}$ phases are found in $x = 12.5$ films, while Sb_2Se_3 is the other major phase revealed from x-ray diffraction studies. The optical gap remains constant at 1.55 eV for $x = 10, 11$ samples and then decreases to 1.50 eV for the $x = 12.5$ film, while a blueshift in reflectivity maxima (R_{max}) has been observed with Sn content. An increase in room temperature conductivity and a decrease in dc activation energy with Sn content have been observed. Bimolecular recombination is the dominant recombination process under steady state illumination for all of the samples. Decay of photocurrent (after cessation of light) fits well to a stretched exponential function; the decay time constant and dispersion parameter have been discussed. The growth of network connectivity with an increase in compositional/configurational disorder induces states in the mobility gap and affects the structure of band tails. These results have been interpreted in the light of the barrier cluster model developed for chalcogenide glasses.

1. Introduction

Rigidity transitions in network glasses/semiconductors have been observed to influence the physical properties in an anomalous way: existence of an intermediate phase in [1–4] network glasses ($2.4 < Z < 2.67$), where the system self-organizes to minimize the stress [1–4]. The non-reversing enthalpy near the glass transition has a deep global minimum within which the glass transition is thermally reversing or has a minimal ageing effect, which is very important in the design of optical devices [4]. Immiscibility in the mixing of different molecular clusters/units leads to the nanoscale phase separation of the network. Measurement of the properties of these glassy systems in the enlarged 'Z' range has been a subject of many studies. Understanding the role of phase separation on the photo-response behavior is of particular interest in the development of optical components. Growth of a new structural entity in the network influences both the mechanical as well as electronic structure of these materials. For tailoring the properties of these materials for device applications, it is therefore of utmost importance to know completely the influence of these structural modifications on the electronic structure of these materials.

The change in structural disorder with phase separation leads to a change in electronic structure of the material. Investigation of the glass forming region and composition dependence of some physical properties of the Sn–Sb–Se system has increased recent interest due to its probable application for optical power transmission devices in the far-IR region [5, 6]. This system undergoes phase separation that occurs very near to the rigidity percolation threshold ($Z > 2.40$) [5]. This is supposed to create new defect states in the mobility gap with a change in short/medium range order. The effect of structural disorder is more on the conduction band as compared to the valence band; therefore, a larger number of electrons are trapped in localized states near to the conduction band [7]. Measurement of photoconductivity is an important tool for knowing the nature of recombination and defect states in the mobility gap of these semiconducting materials [8–12]. Importantly, photocurrent

decay exhibits a stretched exponential function giving two important parameters, namely characteristic decay constant (τ) and dispersion parameter (α), along with photosensitivity (S) and recombination parameter (γ) which are useful in discussing the recombination processes in these materials. Growth of different molecular clusters in a narrow composition window influences electronic structure without causing much change in the chemical environment in this system. We have therefore studied the effect of phase separation on photoelectrical properties in Sn–Sb–Se glassy films for the first time. Different theories developed for the analysis of photoconduction processes have been used to discuss the present results.

2. Experimental details

Bulk glasses of the $Sn_xSb_{20}Se_{80-x}$ ($x = 10, 11, 12.5$) system were prepared by the conventional melt quenching technique [5]. Deposition was carried out in a high vacuum ($\sim 10^{-5}$ Torr) by using a HINDHIVAC coating unit (model no. 12A4D). Well-cleaned glass substrates kept at room temperature as substrates and source material taken in molybdenum boats were used for the deposition. After the deposition, films were kept inside the vacuum chamber for 24 h to attain metastable equilibrium as suggested by Abkowitz [13]. The thickness of the films was measured by using a surface profiler (KLA Tencor P15) and found to be ~850 nm. Thin film samples were annealed at their peak crystallization temperature for 1 h in a running vacuum $\sim 10^{-5}$ Torr. The amorphous/crystalline nature of the samples was confirmed by using a PANalytical X'pertPRO system. The amorphous nature of as-prepared films was confirmed by the absence of any sharp peak in the diffraction patterns. Composition of the pristine and annealed films was checked using a scanning electron microscope (Philips XL30 ESEM system with EDAX attachment) operated at 20 kV. The elemental composition (Sn, Sb and Se) for each film was measured at three different points and the average value taken is found to be within ~2% accuracy as compared to that of the bulk samples.

Transmittance (T) and specular reflectance (R) of the films were carried out by using a UV–VIS–NIR spectrophotometer (Varian Cary 500) in the wavelength range 200–2500 nm. The Al electrodes (electrode gap ~2 mm) in co-planar geometry were used for electrical measurements. Before the electrical measurements, the samples were annealed at 353 K, well above the temperature range of measurements and below their glass transition temperature for 30 min. The dc conductivity measurements were carried out in the temperature range 253–343 K in a running vacuum of $\sim 10^{-4}$ mbar. The current was measured using a digital picoammeter (DPM-111, Scientific Equipment, Roorkee). A 500 W tungsten halogen lamp (Halonix, India) with a heat-absorbing filter was used to illuminate the films. By changing the distance between the sample and light source, intensity was varied and measured through a digital lux meter (LX-102, Taiwan). Least-squares curve fitting was used to estimate the errors in the present work.

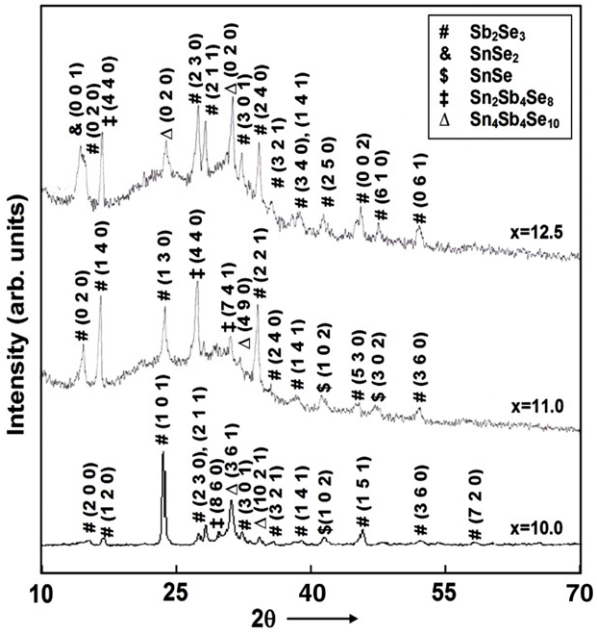

Figure 1. X-ray diffraction patterns for devitrified $Sn_xSb_{20}Se_{80-x}$ glassy films.

3. Results and discussions

3.1. Structure of thin films

The amorphous nature of as-prepared films was confirmed by the x-ray diffraction (XRD) studies (not shown here). The study of devitrified glassy films is important from a fundamental point of view as it provides insights about the relationship between a glass and its corresponding crystalline structure. Figure 1 shows the diffraction patterns for the devitrified (crystallization temperature determined for the bulk glasses using the DSC thermograms) $Sn_xSb_{20}Se_{80-x}$ films. Diffraction peaks for crystallized samples were indexed with Sb_2Se_3 (15-0861), $SnSe_2$ (23-0602), SnSe (32-1382), $Sn_2Sb_4Se_8$ (36-1206) and $Sn_4Sb_4Se_{10}$ (36-1207) phases (JCPDS database, 1997). For $Sn_{10}Sb_{20}Se_{70}$ films, the major phase crystallized is Sb_2Se_3, while some minor peaks were observed for other phases. The relative change in intensity corresponding to different crystallized phases has been observed with Sn content. The segregation of the peak at $2\theta = 15.0°$ for $x = 11$ into two new peaks at $2\theta = 14.4668$ ($SnSe_2$) and 15.0613 (Sb_2Se_3) and dominant peaks for new phases $Sn_2Sb_4Se_8$ (16.8588) and $Sn_4Sb_4Se_{10}$ (23.8177, 31.1485) have been revealed for $x = 12.5$ films. Phase separation occurring in a narrow composition window were discussed elsewhere with a broadening of exothermic peaks for bulk powdered samples [5]. However, the increase in Sn content leads to a decrease in glass transition temperature and thermal stability for bulk glasses. Deterioration of Sb-rich clusters or the Sb_2Se_3 phase lessen their corresponding diffraction peaks, as the accretion of Sn in the Sb_2Se_3 phase leads to dissolution into smaller units, which augment the intensity of new phases for the $x = 12.5$ film sample.

Table 1. Summary of calculated parameters such as optical gap (E_{opt}), activation energy (ΔE) in dark and under illumination, room temperature conductivity (σ_{RT}), photosensitivity (S), recombination parameter (γ), decay time constant (τ) and dispersion parameter (α), with average coordination number (Z) for $Sn_xSb_{20}Se_{80-x}$ glassy films.

			ΔE (±0.02 eV)					B.V. = 10 V		B.V. = 90 V	
x	Z	E_{OPT} (eV)	Dark	Photo	σ_{RT} ($\times 10^{-7}$ S cm^{-1})	S	γ	τ (s)	α	τ (s)	α
10.0	2.40	1.54	0.48	0.11	1.12	0.18	0.52	6.47 ± 0.23	0.37 ± 0.02	10.72 ± 0.32	0.33 ± 0.01
11.0	2.42	1.55	0.41	0.18	1.96	0.04	0.53	0.17 ± 0.01	0.73 ± 0.01	0.38 ± 0.02	0.84 ± 0.01
12.5	2.45	1.50	0.37	0.21	6.53	0.03	0.70	1.42 ± 0.19	0.72 ± 0.02	2.05 ± 0.24	0.77 ± 0.02

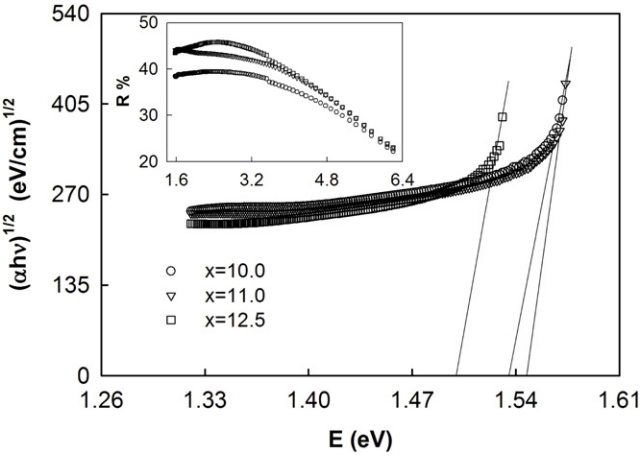

Figure 2. Tauc's plots between $(\alpha h\nu)^{1/2}$ versus $h\nu$ for as-prepared $Sn_xSb_{20}Se_{80-x}$ glassy films. The inset picture shows reflectivity spectra above the fundamental absorption region.

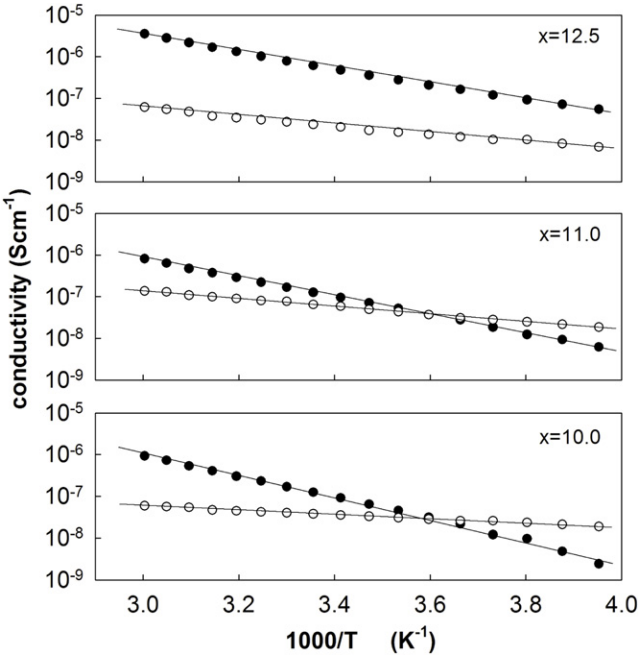

Figure 3. Plots of dark conductivity (filled symbols) and photoconductivity (open symbols) with inverse temperature for $Sn_xSb_{20}Se_{80-x}$ glassy films.

3.2. Optical properties

From the transmission and reflection spectra, the absorption coefficient (α) of the films has been calculated by using the relation [14]

$$\alpha = \left(\frac{1}{t}\right) \ln\left\{\frac{(1-R^2)}{(2T)} + \left\{\frac{(1-R^2)}{(2T)^2} + R^2\right\}^{1/2}\right\} \quad (1)$$

where t is the thickness of films, and T and R represent the transmittance and reflectance, respectively. The absorption coefficient so obtained has been found to lie between 10^4 and 10^5 cm^{-1} near the fundamental absorption region. Figure 2 shows the plots of $(\alpha h\nu)^{1/2}$ versus $h\nu$ for all the films and values of Tauc's gap (E_g) were evaluated from the extrapolation of high energy points to intercept on the energy axis with zero absorption (table 1). A nearly constant value of optical gap (∼1.55 eV) for $x = 10, 11$ and then a decrease to 1.50 eV for $x = 12.5$ in the $Sn_xSb_{20}Se_{80-x}$ samples has been observed. Wakkad *et al* have reported a similar variation in the optical gap for a similar system ($x > 10$) [6]. There is an increase in the average bonding energy with increasing Sn content, but these results can be ascribed to phase separation of constituents in the network structure for the $x = 12.5$ film sample.

It is difficult to measure the accurate transmission spectra of semiconductor films in the spectral region above the fundamental absorption edge, involving strong interband optical transitions. Reflection spectra in the interband transition region have a broad spectral dependence characteristic of amorphous materials. Increase in reflectivity is due to the increase in the metallic character while the blueshift in the reflectivity maxima (inset of figure 2) with the increase in Sn content has been observed (reflectivity maxima have not been observed for the $x = 11$ film sample). Increase in the average bond energy may lead to this shift.

3.3. Temperature dependence of conductivity

DC electrical conductivity has been measured in the temperature range 258–343 K for as-prepared $Sn_xSb_{20}Se_{80-x}$ samples. Figure 3 shows the variations of $\ln\sigma$ with inverse temperature $1/T$ in the dark as well as with illumination (intensity = 1200 lx). Linearity of these plots indicates that the conductivity is thermally activated in the studied temperature region. Dark conductivity and photoconductivity (σ) follow the relation: $\sigma = \sigma_o \exp(-\Delta E/kT)$, where σ_o is a pre-exponential factor, ΔE is the activation energy and k is the Boltzmann constant [7, 11]. Table 1 summarizes the values of activation energies (ΔE) in the dark and under illumination conditions (1200 lx) which have been estimated

from the slope of curves by computer fitting. Decrease in dc activation energy or increase in room temperature conductivity may be due to an increase in carrier concentration or enhancement in metallic behavior with Sn content [7]. Activation energy for photoconductivity was found to be less than that for the dark conductivity value as reported for other chalcogenide semiconductors [11, 15]. An inverse trend in activation energies in the dark and photoconductivity has been observed with composition. No peak in the temperature versus photoconductivity plots has been observed and a lower value of photoconductivity than for the dark conductivity categorizes this system as a type II photoconductor [15].

3.4. Photocurrent measurements

Figure 4 shows a plot of time versus normalized photocurrent (normalized to its maximum value) at 1200 lx light intensity at two different bias voltages namely 10 and 90 V for amorphous $Sn_xSb_{20}Se_{80-x}$ ($x = 10, 11, 12.5$) films. No photodegradation was observed during illumination and reaches a steady state value in a monotonic manner for all the samples. A steep rise in the photocurrent for $x = 11$ and a slow rise for the other films ($x = 10, 12.5$) was observed. After cessation of illumination, photoconductivity decay is quite fast in the initial stage followed by a non-exponential decay for all samples. Decay of the photocurrent reveals a persistent current, i.e. the photoinduced effect persists for a long time prior to reaching its dark equilibrium value [10]. The persistent current was least for $x = 11$. Change in bias voltage results in similar trends in the present work. In these materials, the recombination time of carriers is the same as the carrier lifetime, when the free carrier density is more than the trapped carriers. Otherwise, the recombination process is dominated by the rate of trap emptying and is much larger than the carrier lifetime, resulting in the slow decay [9]. Persistent photocurrent increases with the increase in bias voltage and is found to be largest for the $x = 10$ film samples. An increase in bias voltage leads to an increase in equilibrium thermal carriers along with a change in the density/distribution of defect states, leading to a decrease in photosensitivity and a change in recombination processes [11]. This also leads to an enhancement in deep trapping states and the rate of de-trapping now governs the recombination process and results in an increase in persistent photocurrent with the increase in bias voltage in the present work. To make analysis more precise, the persistent photocurrent is subtracted from the measured total photocurrents. One of the important parameters in photoconductivity analysis is photosensitivity ($S = I_{ph}/I_d$) at a particular temperature, intensity and bias conditions. Values of photosensitivity at room temperature with 10 V biasing are summarized for all samples in table 1. The increase in dark conductivity may also be the reason for the observed decrease in photosensitivity with composition and bias voltage conditions.

Photocurrent relaxation in amorphous chalcogenides has gained a satisfactory interpretation in the framework of the model of multiple trapping in gap states, quasi-continuously distributed in the mobility gap of an amorphous semiconductor as proposed by Iovu *et al* [8, 9]. The study of decay

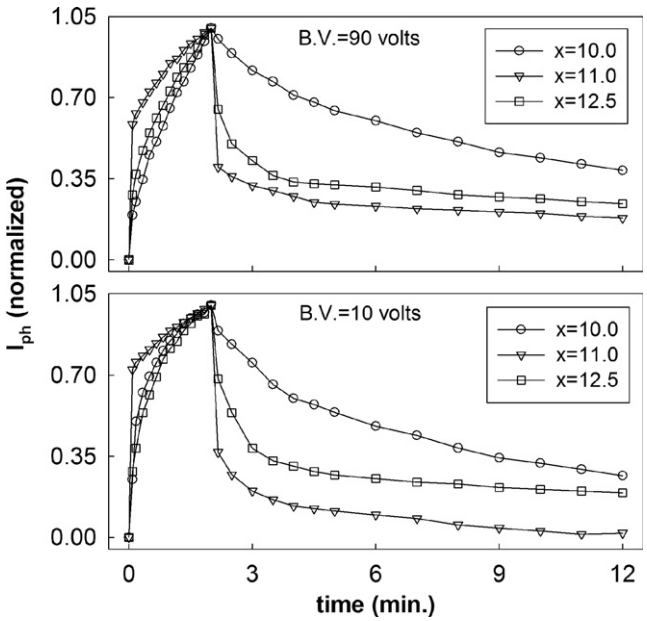

Figure 4. Rise and decay of normalized photocurrent with time at different bias voltages 10 and 90 V for $Sn_xSb_{20}Se_{80-x}$ glassy films.

rates upon switching off the light source is more informative and revealing, especially in terms of relaxation processes prevailing in the system. Non-exponential relaxation of photoconductivity is typical for the majority of amorphous semiconductors and is usually attributed to a wide spectrum of localized states in the gap [8–12, 16]. It is generally assumed that, after light cessation, photocurrent decays due to the capture of non-equilibrium charge carriers (holes) by band tail localized states and, later on, due to recombination.

Data of the photocurrent after the cessation of light has been well fitted to a stretched exponential function of the type $I_{ph}(t) = I_{ph}(0)\exp[-(t/\tau)^{\beta}]$, where $I_{Ph}(0)$ is the photocurrent buildup level at the moment that light excitation is removed, τ is the characteristic decay time and $0 < \beta < 1$ is the stretching exponent, which can be related to the dispersion parameter α ($\alpha = 1 - \beta$) [12]. It indicates the degree of disorder and is associated with a distribution of activated energies for a material. The use of this model leads to an interpretation which demands that the physical nature of the recombination changes with time, spanning over large timescales. Figure 5 shows the plot for the log(normalized photocurrent) with time for the transient decay process. Table 1 shows the fitted values for these parameters at different bias voltages for all the films. These values are in good agreement with those published in the literature [9, 12]. The value of the dispersion parameter $\alpha = 0.37$ for $x = 10$, while its value changes to $\sim$0.73 for $x = 11, 12.5$, while the least value of decay time (τ) for $x = 11$ film and larger value for $x = 10$ films has been found. A similar trend in the relaxation parameters has been observed for higher values of bias voltage (90 V). This increase can be attributed to an increase in field-induced deep defect states which restrict the decay process to longer time constants. A large value of persistent photocurrent and small photosensitivity along with very long decay times for $x = 12.5$

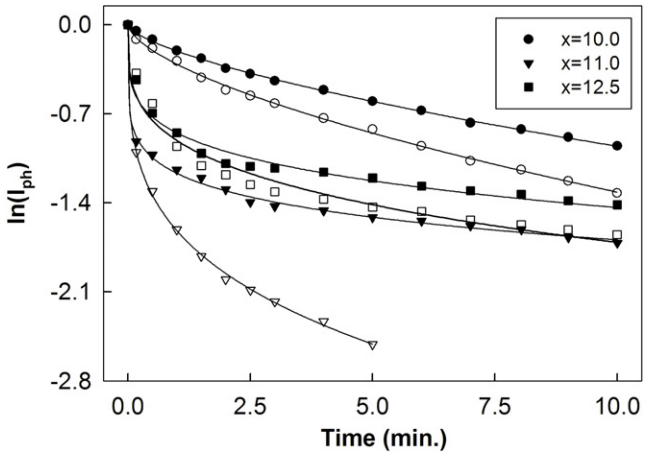

Figure 5. Normalized photocurrent decay (open and full symbols represent the measurements at 10 V and 90 V bias voltage conditions, respectively) curves for $Sn_xSb_{20}Se_{80-x}$ glassy films. Solid curve represents the least-squares fit for photocurrent decay data by a stretched exponential function.

suggests an increase in the trapping states or retardation of the recombination process. These results are also supported by the transient behavior of the photocurrent rise during illumination.

Intensity dependence of photoconductivity has also been studied for different film samples. This obeys the power law $I_{ph} \propto F^{\gamma}$, where I_{ph} is the photocurrent, F is the light intensity and γ is the exponent that determines the recombination mechanism [10, 11, 15]. The value of $\gamma = 0.5$ indicates a bimolecular recombination mechanism, whereas $\gamma = 1.0$ indicates a monomolecular recombination mechanism. If the value of the exponent lies between 0.5 and 1.0, an exponential distribution of traps is present in the gap. Its value for all the samples is summarized in table 1. Thus, bimolecular recombination is the key process governing the recombination under steady state conditions in the present case.

3.5. Barrier cluster approach

The present results can also be discussed in the light of the barrier cluster model used to elaborate the majority of electronic and optical phenomena in network glasses [17, 18]. It considers the potential barrier that arises due to clusters, and tunneling of carriers through these barriers occurs due to the absorption of light in the region of the optical absorption edge at low temperatures. Due to this, the absorption process is influenced by barriers and hence the photoconductivity parameters. However, phase separation is observed in the narrow composition window without much change in the chemical structure and thus their growth can be discussed using this model.

Decrease in dc activation energy and room temperature dc conductivity value suggests an increase in charge carrier concentration or an increase in the localized state density with composition. However, a larger value of dispersion parameters along with a small value of the decay constant and a smaller value of persistent photocurrent for $x = 11$ has been observed. As Sn content increases, the growth of different molecular clusters leads to phase separation which induces states in the gap of the material. This enhances the density of trapping states in the mobility gap or restricts their recombination processes which can be associated with a change in barrier potentials linked to these units. This results in an increase in both the persistent photocurrents and a decrease in the photosensitivity for the $x = 12.5$ film sample. A large value of persistent photocurrent observed for $x = 12.5$ might be connected to the capture of excited photocarriers by deep traps, which have a lesser probability or a longer time required for recombination. This leads to a change in the recombination exponent (γ) and thus exhibiting an exponential distribution of states in the mobility gap. Although the structure of chalcogenide films is supposed to consist of different microregions or clusters having the same structure and physical properties, these results suggest the importance of the growth of clusters in tailoring the physical properties of these network systems. The composition $x = 10$ (or $Z = 2.40$) is at the rigidity threshold for this system and thus a large value of persistent photocurrent and photosensitivity can be ascribed to some photostructural transformations during light illumination, leading to a large value of decay time constant. As the Sn content increases ($x = 11$), the network stiffens, giving a small value of different dispersion parameters along with a small value of photosensitivity. Further addition of Sn leads to an increase in dispersion parameters with decreasing photosensitivity, which can be ascribed to the effect of phase separation in this network system. This increase is associated with the interaction of photo-generated carriers with clusters boundaries due to the phase separation in this system.

4. Conclusions

The effects of phase separation on the optical gap, dc activation energy and photoelectrical properties of thermally evaporated $Sn_xSb_{20}Se_{80-x}$ ($x = 10, 11, 12.5$) films have been discussed. Conductivity parameters and optical gap decrease with the increase in Sn content. Phase separation leads to an increase in the density of deep traps and affects the photocurrent behavior in the studied system. Photosensitivity is found to decrease with composition and bias voltage conditions, while bimolecular recombination is the dominant recombination process during the steady state for all samples. Fitting of post-transit photocurrent data in the stretched exponential shows the dispersive monomolecular transport process during the decay process. Characteristic decay constants and dispersion parameters have also been reported for this system. These results have been discussed in view of the barrier cluster model developed for the network systems.

Acknowledgments

One of the authors (PK) is grateful to the financial assistance provided by the CSIR, New Delhi (India) through SRF (Ext.). We are also grateful to the SAIF/CIL, Punjab University, Chandigarh for providing us with the x-ray facility.

References

[1] Boolchand P 2000 *Insulating and Semiconducting Glasses* (Singapore: World Scientific)

[2] Thorpe M F, Jacobs D J, Chubynsky M V and Philips J C 2000 *J. Non-Cryst. Solids* **266–269** 859

[3] Bresser W J, Suranyi P and Boolchand P 1986 *Phys. Rev. Lett.* **56** 2493

[4] Selvanathan D, Bresser W J and Boolchand P 2000 *Phys. Rev.* B **61** 15061

[5] Kumar P, Kumar J and Thangaraj R 2007 *Eur. Phys. J. Appl. Phys.* **36** 1

[6] Wakkad M M, Shokr E Kh, Abd El Ghani H A and Awad M A 2008 *Eur. Phys. J. Appl. Phys.* **43** 23

[7] Mott N F and Davis E A 1979 *Electronics Process in Non-Crystalline Materials* 2nd edn (Oxford: Clarendon)

[8] Iovu M S, Shutov S D and Popescu M 2002 *J. Non-Cryst. Solids* **299** 924

[9] Iovu M S, Vasiliev I A, Colomeico E P, Emelianova E V, Arkhipov V I and Adriaenssens G J 2004 *J. Phys.: Condens. Matter* **16** 2949

[10] Mehra R M, Ganjoo A and Mathur P C 1994 *J. Appl. Phys.* **75** 7334

[11] Kumar P and Thangaraj R 2008 *J. Phys.: Condens. Matter* **20** 095213

[12] Harea D V, Vasilev I A, Colomeico E P and Iovu M S 2003 *J. Optoelectron. Adv. Mater.* **5** 1115–20

[13] Abkowitz M 1984 *Polym. Eng. Sci.* **24** 1149

[14] Fang F, Li Q and Gan F 2004 *Chin. Phys. Lett.* **2** 177

[15] Bube R H 1992 *Photoelectrical Properties of Semiconductors* (Cambridge: Cambridge University Press)

[16] Andriesh A M, Arkhipov V I, Iovu M S, Rudenko A I and Shutov S D 1983 *Solid State Commun.* **48** 1041

[17] Banik I 2007 *J. Non-Cryst. Solids* **353** 1920

[18] Banik I 2008 *Chal. Lett.* **5** 87